Effect of Cooling Rate on Crystallization Behavior of Milk Fat Fraction/Sunflower Oil Blends

S. Martini[a], M.L. Herrera[a], and R.W. Hartel[b,*]

[a]Centro de Investigación y Desarrollo en Criotecnología de Alimentos (CIDCA) (UNLP-CONICET), La Plata 1900, Argentina, and [b]Food Science Department, University of Wisconsin–Madison, Madison, Wisconsin 53706

ABSTRACT: The effect of cooling rate (slow: 0.1°C/min; fast: 5.5°C/min) on the crystallization kinetics of blends of a high-melting milk fat fraction and sunflower oil (SFO) was investigated by pulsed NMR and DSC. For slow cooling rate, the majority of crystallization had already occurred by the time the set crystallization temperature had been reached. For fast cooling rate, crystallization started after the samples reached the selected crystallization temperature, and the solid fat content curves were hyperbolic. DSC scans showed that at slow cooling rates, molecular organization took place as the sample was being cooled to crystallization temperature and there was fractionation of solid solutions. For fast cooling rates, more compound crystal formation occurred and no fractionation was observed in many cases. The Avrami kinetic model was used to obtain the parameters k_n and n for the samples that were rapidly cooled. The parameter k_n decreased as supercooling decreased (higher crystallization temperature) and decreased with increasing SFO content. The Avrami exponent n was less than 1 for high supercoolings and close to 2 for low supercoolings, but was not affected by SFO content.

Paper no. J9999 in *JAOCS 79,* 1055–1062 (November 2002).

KEY WORDS: Avrami equation, cooling rate, crystallization, high-melting milk fat fraction, sunflower oil.

Of the natural fats, milk fat contains the most complex lipid composition. TAG constitute by far the greatest proportion of milk fat, making up 97–98% of the total lipids. The other components include DAG, MAG, FFA, free sterols, and phospholipids. Owing to its complex composition, the melting range of milk fat is broad, from about –40 to 40°C. Furthermore, the composition changes with season, region, and feeding (1). To extend the use of milk fat in food, pharmaceutical, and cosmetic products, fractionation may be performed to produce components with specific properties (e.g., m.p.). Milk fat fractions are also blended to give a manufacturer greater flexibility to tailor milk fat ingredients to specific functional requirements than could be accomplished with fractionation alone (2).

Milk fat fractions find increasing application in a variety of food products (3). Modification of high-m.p. stearins by blending with vegetable oils is becoming important, because shortenings with good nutritional properties that are free of *trans* FA and rich in PUFA can be obtained. Roy and Bhattacharyya (4) simulated a hydrogenated fat product by blending palm stearins with liquid oils, such as sunflower, soybean, and rapeseed. Pal *et al.* (5) modified butter stearin by blending it with sunflower oil (SFO) and soybean oil to make fats with desired physical properties and FA compositions suitable for utilization in a variety of food products.

Understanding the effects of formulation and process factors on the kinetics of crystallization is important for control of product quality. Isothermal crystallization, as measured by NMR, has been performed on milk fat and its fractions as well as on other fat systems (6–9). However, the effect of cooling rate has not been previously investigated by NMR. All the reported studies were performed by quenching a melted fat to crystallization temperature.

Many factors influence lipid crystallization, most notably the way in which the sample is cooled from the melt (cooling rate, initial and final temperatures, agitation rate), and composition (FA profile and TAG organization) (10). The present work investigated the effects of cooling rate on crystallization kinetics and thermal behavior of blends of a high-melting milk fat fraction with SFO. The Avrami model was used to interpret the isothermal behavior of rapidly cooled blends, and kinetic parameters, such as crystallization rate (k_n) and the Avrami coefficient (n), were calculated.

MATERIALS AND METHODS

Starting materials. High-melting milk fat fraction (HMF) was obtained from La Serenisima S.A. (Gral. Rodriguez, Buenos Aires, Argentina) and SFO from Molinos Rio de La Plata S.A. (Avellaneda, Buenos Aires, Argentina). Three blends were prepared by mixing 10, 20, and 40% of SFO with HMF. Dropping points of the samples were determined with the Mettler FP 80 Dropping Point Apparatus (Mettler Instruments A.G., Greifensee-Zurich, Switzerland), using a heating rate of 1°C/min.

GC analysis. Acyl carbon profile of samples was determined with a Hewlett-Packard 5890 Series II (Hewlett-Packard, San Fernando, CA) GC unit equipped with an FID and on-column injector. The column used was a Heliflex Phase AT-1 with a length of 30 m and an internal diameter of 0.25 mm (Alltech Associates, Deerfield, IL). Helium was the carrier gas at a flow rate of 2 mL/min, with hydrogen gas and air also being supplied to the FID. Samples were prepared by

*To whom correspondence should be addressed at Food Science Department, University of Wisconsin–Madison, 1605 Linden Dr., Madison, WI 53706. E-mail: Hartel@calshp.cals.wisc.edu

using a modified method of Lund (11). A 10-mg sample was weighed in GC vials and dissolved in 1.8 mL of isooctane with 100 μL of internal standard (C_{27} in isooctane: 2.02 mg/mL). Samples were stored in a refrigerator prior to analysis. To separate the different TAG according to acyl carbon number, the following temperature profile was used in the GC: initially hold at 280°C for 1 min, and then increase at a rate of 3.0°C/min until a temperature of 355°C is reached. The detector was held constant at 370°C. Composition was based on the area integrated by using ChemStation Chromatography software by Hewlett-Packard and reported as a percentage of the total peak area. Samples were run in duplicate.

Equilibrium solid fat content (SFC) determination. SFC of the fully crystallized samples were measured by pulsed NMR (p-NMR) in a Minispec PC/120 series NMR analyzer (Bruker, Karlsruhe, Germany). The blends of HMF with 10, 20, and 40% SFO were tempered according to the AOCS temperature treatment (12) to ensure full crystallization. Samples were run in duplicate and the values were averaged.

Crystallization studies. Crystallization was performed by using the following thermal treatments: Samples were melted at 80°C for 30 min, and then the NMR tubes were filled with the samples, kept at 80°C for another 30 min, and then (i) immediately placed at crystallization temperature (T_c) (fast rate) or (ii) cooled from 60°C to T_c at 0.1°C/min using a programmable Lauda ethyleneglycol/water (3:1) bath model RK 8 KP (Werklauda, Königshofen, Germany) (slow rate). The fast cooling rate was calculated from the initial slope of the temperature record of the NMR tube, as measured by a copper-constantin thermocouple. The results of several runs were averaged to obtain an average cooling rate of 5.5 ± 0.2°C/min. The selected crystallization temperatures (T_c) were 5, 10, 15, 20, 25, 30, and 35°C for both cooling rates. For the slow cooling rate, SFC was measured during cooling as well as during the isothermal hold at crystallization temperature. For fast cooling, SFC measurements started when the isothermal crystallization temperature was reached (denoted as time zero). In both cases, SFC was measured for 3 h after the isothermal crystallization temperature was reached. Results are the average of three runs.

Data analysis. The data were fitted to the Avrami equation (Eq. 1) (13):

$$-\ln(1 - f) = k_n t^n \quad [1]$$

where t is time, k_n is the rate constant, f is the fractional extent of crystallization at any time, and n represents the index of the reaction. The fractional extent of crystallization was taken as the SFC at any given time normalized by the maximum SFC obtained at that experimental condition. To obtain the parameters that gave the best fit to Equation 1, the nonlinear section of the Systat software was used (Systat, Inc., Evanston, IL). Statistical significance of differences in parameters k_n and n with supercoolings and between samples was checked using ANOVA. A randomized block design and an additive model that assumes that an observation, γ_{ti}, can be represented as the sum of a general mean η, a block effect β_i, a treatment effect τ_t, and an error ε_{ti} were selected (14). Significance of differences in parameters k_n and n for samples with different SFO content was evaluated with this design using crystallization temperature as treatment. A multiple comparisons test was used to determine the confidence interval for a particular difference in means.

DSC. Measurements were carried out in a Polymer Laboratories calorimeter (Rheometric Scientific Ltd., Piscataway, NJ) driven with Plus V 5.41 software. Calibration was carried out at a heating rate of 5°C/min by using indium proanalysis (p.a.), lauric acid p.a., and stearic acid p.a. as standards. Samples were melted at 80°C for 30 min. From 5 to 9 mg of sample was placed in a hermetically sealed aluminum pan, held at 80°C for 30 min and subjected to identical thermal treatments as used for NMR studies (with DSC pans held in vials that were cooled in the same water bath as for the NMR study): (i) immediately placed at crystallization temperature (T_c) with cooling at approximately 5.5°C/min (fast rate), and (ii) cooled from 60°C to T_c at 0.1°C/min (slow rate). After 0, 20, and 120 min at T_c, the samples were heated at a rate of 5°C/min from T_c to 80°C. A single empty pan was employed as a reference. Three replicates were performed for each sample to obtain the mean value and a measure of the statistical dispersion of peak temperatures and melting enthalpies.

Polarized light microscopy. A Leitz microscope model Ortholux II (Ernest Leitz Co., Wetzlas, Germany) with a controlled-temperature platform was used to generate images of the fat crystals during isothermal crystallization. The platform temperature was controlled by a Lauda TUK cryostat (Werklauda). Photographs of the crystals were taken with a Leitz-Vario-Orthomat camera under polarized light. Magnification of 250× was used for all photographs.

X-ray diffraction (XRD). Samples were analyzed for their polymorphic form by using a Philips 1730 X-ray spectrometer fitted with a system for temperature control (Philips Argentina S.A., Buenos Aires, Argentina). The temperature of the sample holder placed within the refraction chamber was controlled through a programmable Lauda UK 30 cryostat (Werklauda). Ethylene glycol in water (3:1, vol/vol) was used as coolant. $K_{\alpha 1 \alpha 2}$ radiation from copper was used at 40 kV, 20 mA, and a scanning velocity of 1°/min from 5 to 30°C.

RESULTS AND DISCUSSION

Analysis. The m.p. (T_m), measured as Mettler dropping points, and TAG composition of the HMF, SFO, and the three blends are reported in Table 1. T_m of the HMF was 40.2°C and addition of 10% SFO had no effect on m.p. Addition of 20% SFO decreased T_m by 1.4°C, and addition of 40% SFO decreased the m.p. of the mixture by less than 3°C.

Despite the small changes in T_m due to addition of SFO, the SFC curves of the blends decreased substantially as SFO content increased (Fig. 1). At the addition of 40% SFO to HMF, the m.p. decreased by only a few degrees, but the SFC decreased by nearly 50% at all temperatures. Thus, the SFO caused a substantial dilution of the crystalline content of

TABLE 1
Chemical Composition and Mettler Dropping Points (MDP) of Starting Materials and Blends of Sunflower Oil (SFO) in High-Melting Milk Fat Fraction (HMF)

	Chemical composition of starting materials				
Acyl carbon number[a]	SFO	HMF	10% SFO	20% SFO	40% SFO
C26	0.3	0.5	0.5	0.4	0.4
C28	0.0	0.5	0.5	0.4	0.4
C30	0.0	1.0	0.9	0.8	0.7
C32	0.0	2.1	2.0	1.8	1.4
C34	0.0	4.8	4.4	3.9	3.2
C36	0.3	8.6	7.9	7.2	6.3
C38	3.9	13.2	12.4	11.4	7.8
C40	0.0	8.0	7.3	6.6	7.2
C42	0.0	7.0	6.1	5.5	4.2
C44	0.0	7.5	6.5	5.8	4.8
C46	0.0	9.0	6.6	6.9	5.8
C48	0.1	11.0	10.0	8.3	6.8
C50	2.2	13.2	12.5	10.3	8.8
C52	20.1	9.2	10.0	9.9	13.1
C54	73.1	4.3	12.5	20.6	29.3
C54 (18:0)-d	0.8	0.3	1.4	0.3	0.5
C54 (18:1)-a,b,c	72.3	3.9	11.1	20.3	28.8
C54-b (unknown)	4.8	1.5	1.0	2.6	3.1
C54-c (unknown)	0.0	1.0	1.9	0.9	0.4
C54 (18:1*cis*)-a	67.8	1.5	8.1	16.9	25.3
MDP (°C)		40.2	40.4	38.8	37.4

[a]a, b, c, and d indicate individual peaks within the C54 group.

HMF but had only a small effect on the final melting temperature of the highest-melting TAG.

Effect of cooling rate on crystallization by NMR. Figure 2 shows the increase in SFC with time for the samples crystallized at slow rate (0.1°C/min). Zero time for these graphs was the moment at which the samples reached crystallization temperature. For the slowly cooled samples crystallized at temperatures of 5, 10, 15, and 20°C, the initial solid content was at least 90% of the final solid content (after 200 min), indicating that most of the crystallization took place before the temperature reached the designated crystallization temperature. At 35 and 30°C, a short induction period was necessary to start crystallization for all samples. At 25°C, addition of 20 and 40% SFO (Figs. 2C,D) resulted in slower crystallization, where a rapid increase in SFC during the first 30 min after reaching crystallization temperature was observed. The HMF by itself and 10% SFO sample were essentially fully crystallized when the temperature reached 25°C. As expected, the final SFC (after 180 min) decreased as crystallization temperature increased, indicating the decrease in crystalline phase volume as temperature increased. Furthermore, increased levels of SFO caused a decrease in SFC for any given crystallization temperature, as predicted by the decrease in SFC in the NMR curves (Fig. 1). Thus, addition of SFO resulted in a slower crystallization rate and decreased the phase volume of HMF under these conditions, with greater effect at higher levels of SFO addition.

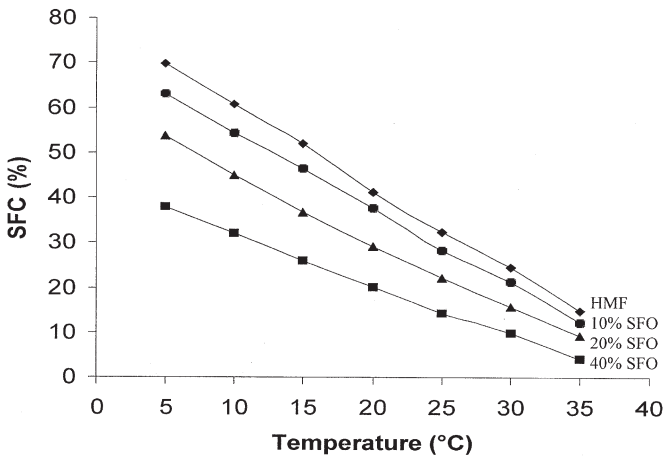

FIG. 1. Solid fat content (SFC), as measured by pulsed NMR, of mixtures of high-melting milk fat fraction (HMF) with sunflower oil (SFO).

The thermodynamic driving force is one factor that influences the rate of crystallization. However, other processing factors, such as heat and mass transfer during processing, also can have significant effects on the rate of crystallization. For example, the manner by which the thermodynamic driving force for crystallization is achieved and the rate of development of this driving force determine the rates of formation and growth of crystals (15). In particular, the rate of cooling can substantially influence crystallization rates. At slow cooling rates, molecular organization takes place as the sample is slowly being cooled to crystallization temperature. Typically, fewer crystals of higher purity are obtained in this case. In contrast, rapid cooling forces the molecules to organize into crystals under conditions farther from equilibrium. Faster cooling generally results in more compound crystal formation (lower purity) and higher SFC at any crystallization temperature compared with slower cooling. Comparison of Figures 2 and 3, particularly at crystallization temperatures below 25°C, shows that there is a higher SFC for samples cooled quickly than for those cooled slowly. At higher crystallization temperatures (lower supercooling), the SFC is about the same for both cooling rates.

Crystallization with fast cooling (Fig. 3) also showed a different behavior from that for slow cooling (Fig. 2). For fast cooling at crystallization temperatures below 25°C (0, 10, and 20% SFO) and 20°C (40% SFO), there was no induction time of crystallization, and curves showed a hyperbolic shape. However, a slight plateau in SFC was visible in all curves. The SFC at the plateau decreased steadily both in rate and height as T_c was increased. The second step of crystallization, above the plateau, was sigmoidal in shape. For low supercoolings (crystallization temperature above 25°C), curves had sigmoidal shapes. At the beginning, there was an induction time when no fat crystallized, which was followed by a period of rapid crystallization. Again, the maximum SFC (S_{max}) decreased with the addition of SFO. At 5°C, the HMF sample had a S_{max} of 74%, whereas addition of 10% SFO reduced S_{max} to only 65%. This decrease in S_{max} occurred even though the T_m was similar for both samples, 40.2 and 40.4°C, respec-

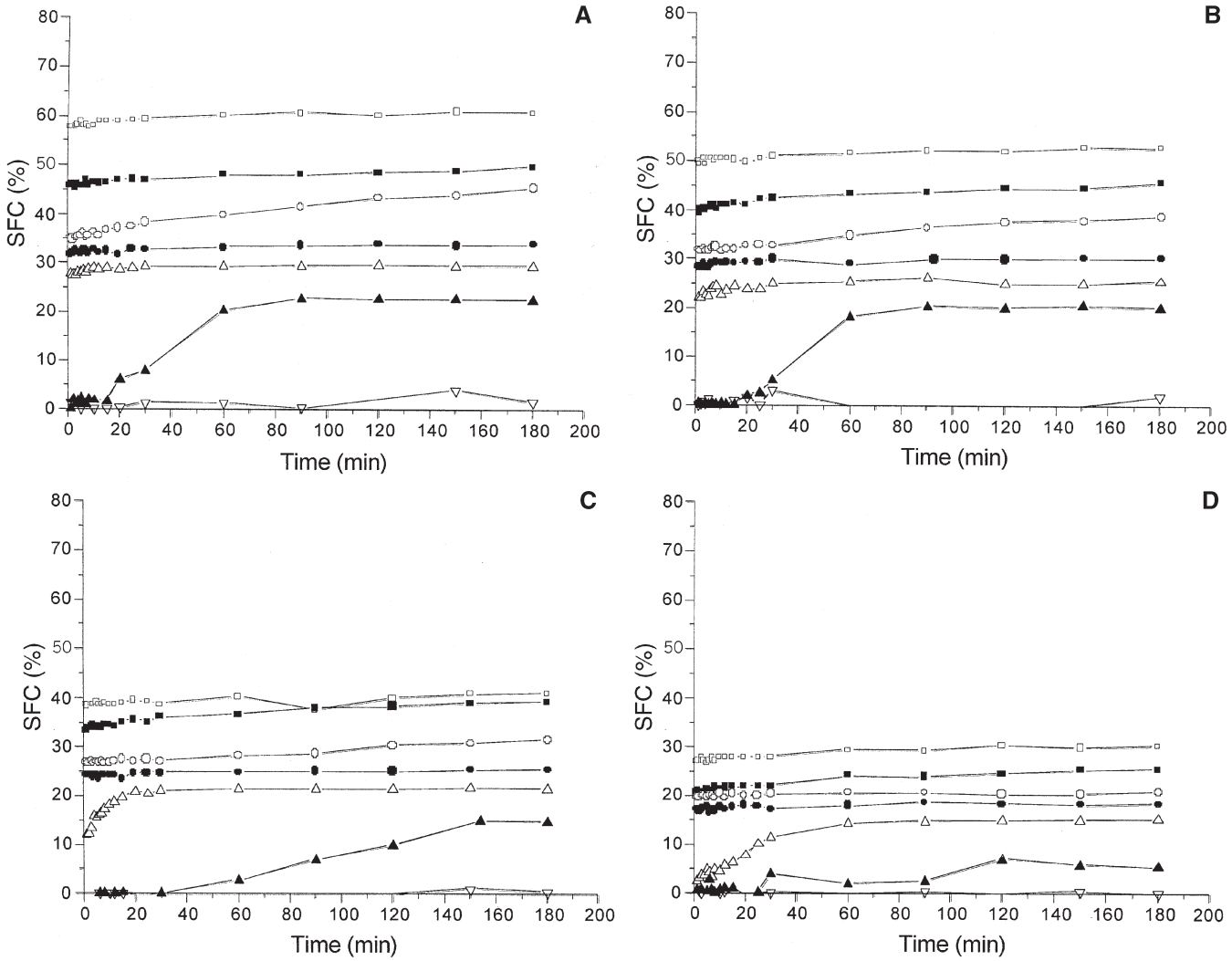

FIG. 2. SFC with time for the samples crystallized at slow cooling rate (0.1°C/min): (A) HMF, (B) 10–90% SFO/HMF, (C) 20–80% SFO/HMF, and (D) 40–60% SFO/HMF. Symbols: □, ■, ○, ●, △, ▲, ▽ at 5, 10, 15, 20, 25, 30, and 35 ºC, respectively. See Figure 1 for abbreviations.

tively. The 40% SFO blend had a T_m of 37.4°C and an S_{max} of 43% at 5°C.

XRD studies. For all samples at all T_c and for both cooling rates, only the β′ polymorph was found. As shown in Figure 4, the XRD patterns were characteristic of the β′ polymorph with two strong signals at 3.8 and 4.3 Å. No signal at 4.6 Å, characteristic of the β-form, was found. X-ray spectra for all samples were very similar and, therefore, polymorphism was not responsible for differences in crystallization behavior.

DSC studies. Figure 5 shows representative DSC thermograms for the HMF and the sample with 40% SFO cooled either rapidly or slowly to 25°C. The thermograms shown correspond to 0, 20, and 120 min (HMF) and 20 and 120 min (the 40% SFO blend) after the samples reached crystallization temperature. For the pure HMF sample, at zero time, the rapidly cooled sample showed a small symmetric peak (Fig. 5A), indicating that a very small amount of crystallization had occurred in this system, whereas the slowly cooled sample showed a larger peak with a shoulder at low temperature (Fig. 5B). Slow cooling promoted crystallization, and thus a higher total enthalpy was obtained at zero time compared with fast cooling. Melting enthalpy was 27.3 ± 2.1 mJ/mg at time zero for slow cooling, whereas it was only 2.25 ± 1.3 mJ/mg for fast cooling. Slowly cooled samples after 20 and 120 min at crystallization temperature had a large endotherm at about 30°C, which increased with time at crystallization temperature (Fig. 5B). This means that with slow cooling, fractionation of the TAG had occurred as was evidenced by the two peaks in the DSC scans, representative of two different solid solutions formed. Total melting enthalpies showed no significant differences between cooling rates for 20 and 120 min ($P < 0.05$). Enthalpies were 25.6 ± 2.1 and 29.9 ± 2.3 mJ/mg after 20 min of crystallization for rapid and slow cooling, respectively, and after 120 min of crystallization, enthalpies were 37.7 ± 2.4 and 34.6 ± 2.4 mJ/mg for rapid and slow cooling, respectively. The samples with 10 and 20% addition of SFO showed behavior similar to that of the pure HMF.

For the sample with 40% SFO, no crystallization had occurred by the time temperature had reached T_c for either slow or fast cooling rates. After 20 min at T_c, small and broad

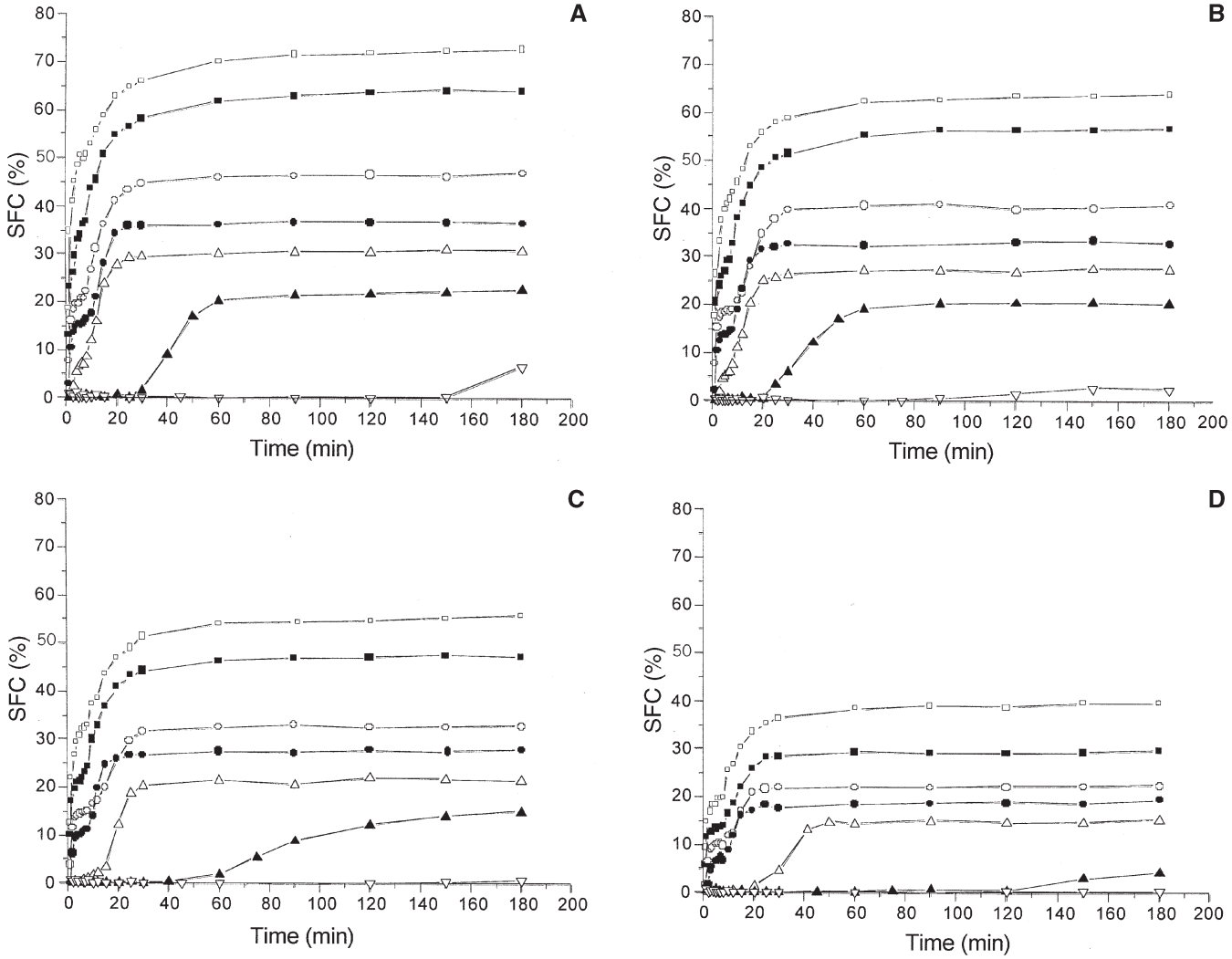

FIG. 3. SFC with time for the samples crystallized at fast cooling rate (5.5°C/min); see Figure 2 for identification of panels A–D and for symbols; see Figure 1 for abbreviations.

peaks were observed in the melting profiles (Figs. 5C,D). Total melting enthalpies for the rapidly and slowly cooled samples were within experimental error (3.3 ± 1.2 and 5.6 ± 2.1 mJ/mg for rapid and slow cooling, respectively). At 120 min, it was clear that slow cooling promoted fractionation, because the low-melting temperature peak was larger and more well-defined than the peaks found for fast cooling. In this case, the total melting enthalpy was higher for slow cooling despite the slightly lower S_{max} measured by NMR (10.9 ± 1.9 and 20.6 ± 2.3 mJ/mg for rapid and slow cooling, respectively). Because the polymorphic form obtained was the same for all blends at all T_c during the 3 h of isothermal crystallization (Fig. 4), the differences found in melting curves were due not to a polymorphic transition but to differences in chemical composition of the crystals formed under these conditions and phase behavior of the mixed TAG.

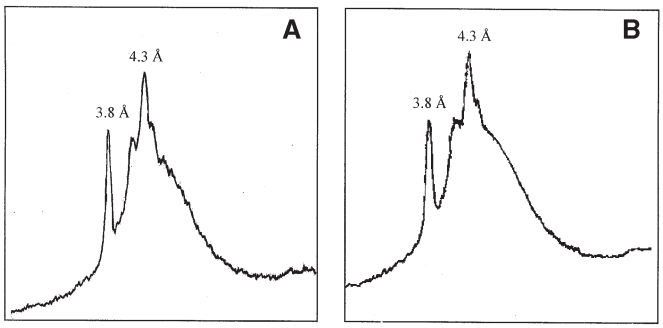

FIG. 4. X-ray patterns of the sample with the addition of 20% SFO collected after 3 h at 35°C. (A) Slow cooling, (B) fast cooling. See Figure 1 for abbreviation.

Initial crystallization during slow cooling. Figure 6 shows how SFC changed with temperature during slow cooling from 80 to 5°C. Clearly, crystallization under these conditions started before the samples reached crystallization temperature. In fact, by the time the temperature reached T_c, the SFC was about 90% of S_{max} in most of the cases. This behavior may be related to the experimental time in which molecular organization took place prior to formation of nuclei. The time scales for nucleation were different between the different cooling rates, and the crystal compositions (and therefore

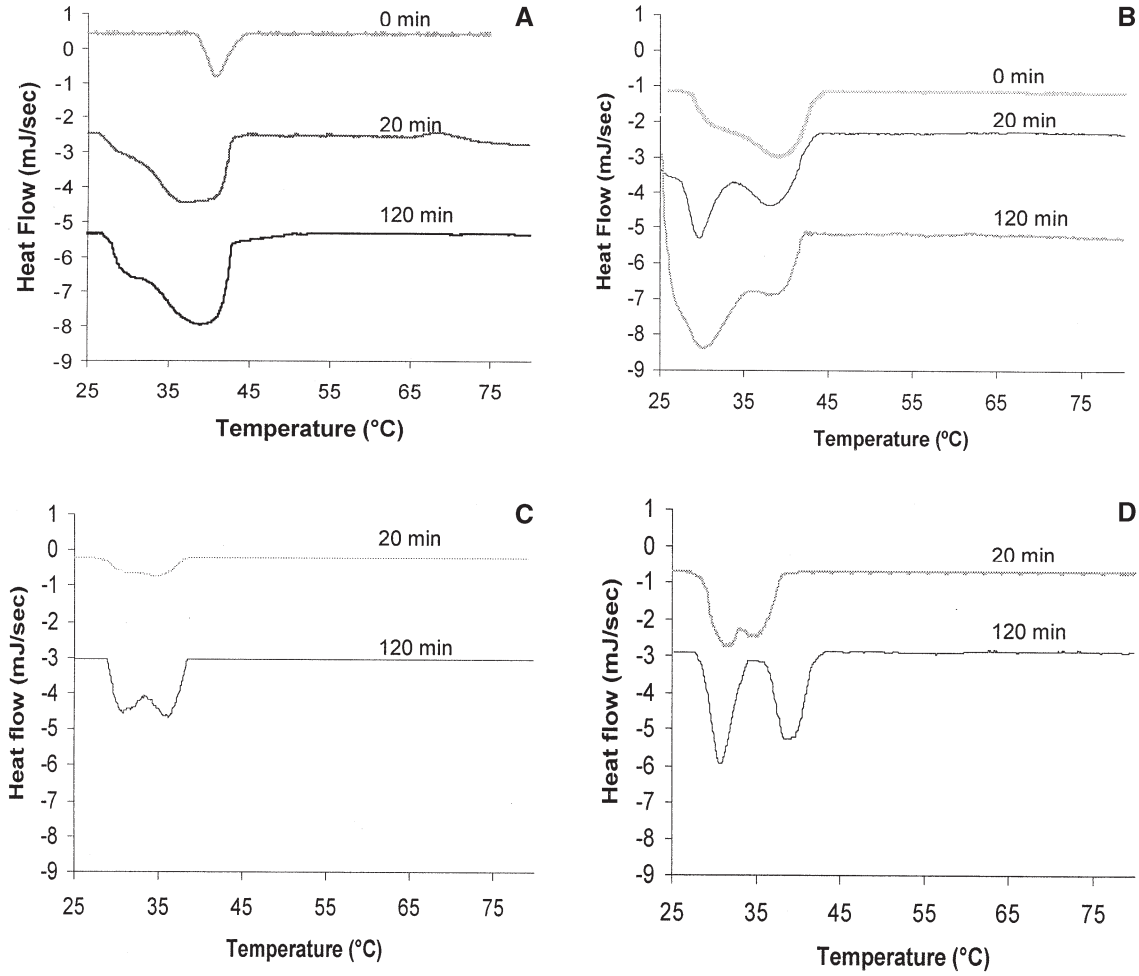

FIG. 5. Melting curves (DSC) for samples cooled to 25°C and held for different times. (A) HMF cooled rapidly (5.5°C/min), (B) HMF cooled slowly (0.1°C/min), (C) 40% SFO in HMF cooled rapidly (5.5°C/min), and (D) 40% SFO in HMF cooled slowly (0.1°C/min). For abbreviations see Figure 1.

melting profiles and SFC curves) of the samples also were different (16).

Two different crystallization regions separated by a plateau zone can be distinguished in Figure 6. The first step occurred in the interval from 30 to 20°C, with the second step occurring in the interval from 15 to 5°C, the limit temperatures of each linear zone being in agreement with the chemical composition of blends (i.e., 30 to 25°C for pure HMF and with the addition of 10% SFO; 30 to 20°C for the 20% SFO blend; and 25 to 20°C for the 40% SFO blend). Selective nucleation occurred at a slow cooling rate, and thus, fractionation of different solid solutions occurred during melting (17).

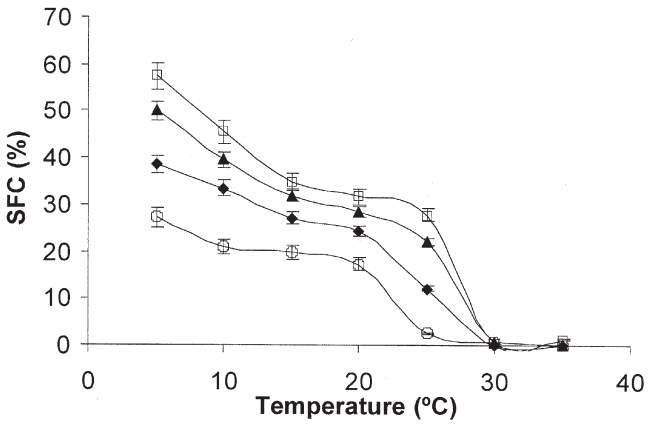

FIG. 6. Change in SFC with temperature during slow cooling. Samples were cooled at 0.1°C/min from 80 to 5°C. □ HMF, ▲ 10% SFO, ◆ 20% SFO, and ○ 40% SFO. For abbreviations see Figure 1.

Rapid cooling: Avrami analysis. For the samples cooled rapidly, an induction time at T_c was observed prior to onset of crystal formation and subsequent increase in SFC. The SFC curves in Figure 3 (fast cooling) were fitted to the Avrami model (Eq. 1) by using a nonlinear regression package, with n values found to fall between 0.4 and 2.6. Table 2 shows k_n values, n values, and the correlation coefficients (r^2) at different temperatures for all samples. There was a good fit over the range of fractional crystallization from 0 to 0.7 as indicated by correlation coefficients and residual analysis ($r^2 > 0.9$ in all cases, Table 2). Not surprisingly, k_n values were higher at lower temperatures ($P \ll 0.001$), indicating that crystallization proceeded more rapidly at higher driving force (lower temperature). For the 0, 10, and 20% SFO addition levels, values of k_n above 25°C were, on average, 10 times lower than at

TABLE 2
Best-Fit Parameters of the Avrami Model (Eq. 1) for Mixtures of SFO in HMF Cooled Rapidly[a] (5.5°C/min)

Blend	Temp. (°C)	k_n (min^{-n})	n	r^2
HMF	5	$2.5 \times 10^{-1} \pm 2.5 \times 10^{-2}$	0.605 ± 0.071	0.997
	10	$1.7 \times 10^{-1} \pm 1.2 \times 10^{-2}$	0.523 ± 0.047	0.998
	15	$1.0 \times 10^{-1} \pm 1.9 \times 10^{-2}$	0.607 ± 0.168	0.991
	20	$5.0 \times 10^{-2} \pm 1.5 \times 10^{-2}$	0.902 ± 0.251	0.984
	25	$2.0 \times 10^{-3} \pm 1.0 \times 10^{-3}$	2.118 ± 0.371	0.971
	30	$4.6 \times 10^{-6} \pm 5.6 \times 10^{-7}$	2.663 ± 0.543	0.973
10% SFO	5	$2.0 \times 10^{-1} \pm 1.1 \times 10^{-2}$	0.587 ± 0.042	0.999
	10	$1.7 \times 10^{-1} \pm 7.5 \times 10^{-3}$	0.406 ± 0.032	0.999
	15	$1.1 \times 10^{-1} \pm 1.6 \times 10^{-2}$	0.411 ± 0.107	0.989
	20	$5.9 \times 10^{-2} \pm 1.6 \times 10^{-2}$	0.580 ± 0.181	0.972
	25	$5.6 \times 10^{-3} \pm 7.7 \times 10^{-4}$	1.330 ± 0.052	0.993
	30	$1.1 \times 10^{-4} \pm 9.9 \times 10^{-6}$	1.872 ± 0.280	0.981
20% SFO	5	$1.6 \times 10^{-1} \pm 1.5 \times 10^{-2}$	0.514 ± 0.067	0.996
	10	$1.2 \times 10^{-1} \pm 1.3 \times 10^{-2}$	0.445 ± 0.086	0.995
	15	$8.0 \times 10^{-2} \pm 9.3 \times 10^{-3}$	0.411 ± 0.039	0.989
	20	$2.7 \times 10^{-2} \pm 6.0 \times 10^{-3}$	0.807 ± 0.087	0.982
	25	$1.8 \times 10^{-4} \pm 4.6 \times 10^{-5}$	2.139 ± 0.292	0.972
	30	$4.2 \times 10^{-5} \pm 8.5 \times 10^{-5}$	1.654 ± 0.258	0.971
40% SFO	5	$1.1 \times 10^{-1} \pm 9.9 \times 10^{-3}$	0.416 ± 0.071	0.996
	10	$7.8 \times 10^{-2} \pm 1.2 \times 10^{-2}$	0.412 ± 0.130	0.988
	15	$3.4 \times 10^{-2} \pm 8.4 \times 10^{-3}$	0.749 ± 0.179	0.984
	20	$8.1 \times 10^{-3} \pm 3.6 \times 10^{-3}$	1.350 ± 0.309	0.974
	25	$1.6 \times 10^{-5} \pm 1.5 \times 10^{-6}$	2.375 ± 0.466	0.974

[a]Temp., temperature; for other abbreviations see Table 1.

lower temperatures. For the 40% SFO blend, this behavior was also shown, but 20°C was the temperature that distinguished the two regions. Slower crystallization of HMF due to addition of SFO was evidenced by the decrease in the parameter k_n at higher SFO levels. At all crystallization temperatures, values of k_n were higher for the pure HMF sample and lower for the sample with 40% SFO. The pure HMF sample had a T_m only 2.8°C higher than the sample with 40% SFO.

The variation of the Avrami parameter k_n with supercooling ($\Delta T = T_m - T_c$) is also shown in Table 2. The Avrami parameter k_n increased with increasing driving force (ΔT) and decreased with increased levels of SFO (at the same ΔT). This suggests that SFO had an inhibiting effect on crystallization of HMF over and above the effect on SFC.

The Avrami exponent, n, shown in Table 2, increased significantly above 25°C for samples with 0, 10, and 20% SFO, and above 20°C for the sample with 40% SFO. The Avrami exponent is a function of the number of dimensions in which growth takes place, and reflects the details of nucleation and growth mechanisms (18). The Avrami equation has been reported to be valid not only for linear growth (i.e., constant growth rate) but also for the early stages of diffusion-controlled growth. Christian (19) has tabulated some values of n that might be expected for various transformation conditions. For example, an n of 4 indicates heterogeneous nucleation and spherulitic growth from sporadic nuclei, whereas an n of 3 indicates spherulitic growth but from instantaneous nuclei. An n of 2 represents high nucleation rate and platelike growth, where growth is primarily along two dimensions. According to the Avrami analysis, two different crystallization mechanisms would be expected below and above the critical temperatures noted above based on the differences in n values. Microscope images of crystals as they formed under these conditions showed clear differences in crystalline microstructure as a function of crystallization temperature (20). Figure 7 shows two images corresponding to the sample with 20% SFO taken at 15 and 30°C. At temperatures above 25°C (low crystallization driving force), Avrami exponents were generally about 2 and crystals formed large spherulite structures. These spherulites were agglomerates of many small needle-shaped crystals (Fig. 7A). In contrast, at temperatures below 20°C (high crystallization driving force), Avrami exponents were generally less than 1 and the crystals appeared as distinct needles with little agglomeration observed (Fig. 7B).

The Avrami exponent n was strongly dependent on supercooling, as seen in Table 2. For low supercoolings ($\Delta T <$ 15°C), n was close to 2, whereas for high supercoolings ($\Delta T >$ 20°C), n was close to 1. However, the Avrami exponent n showed no statistical significance between samples with different SFO blends (at the same ΔT). The addition of SFO apparently did not modify the crystallization mechanism even though crystallization rate was significantly affected.

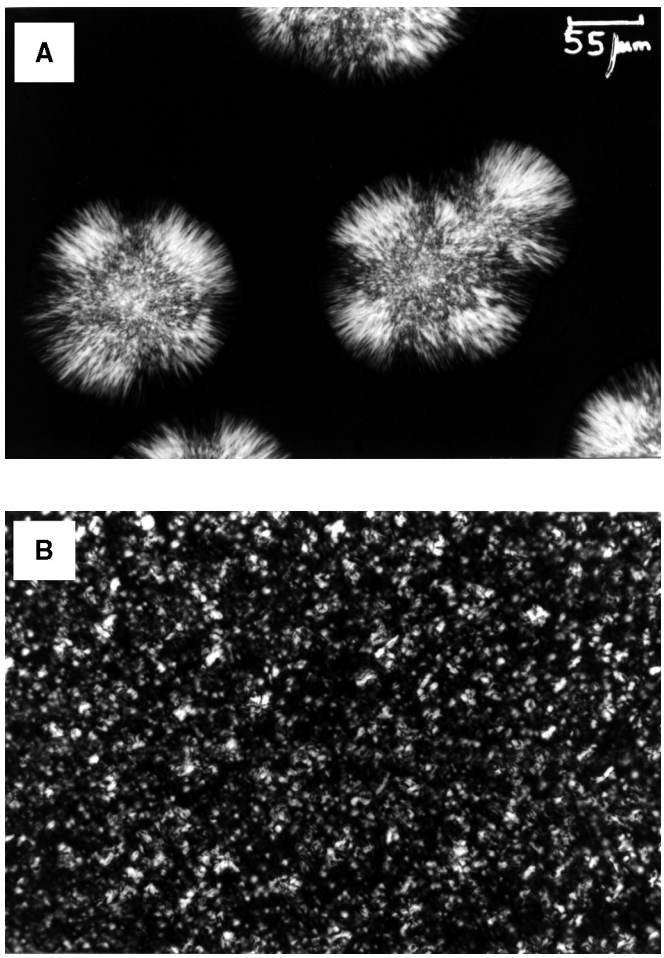

FIG. 7. Photographs (optical microscopy) of the 20% SFO blend cooled rapidly (A) after 90 min at 30°C, and (B) after 40 s at 15°C. Scale in panel B is the same as for panel A. For abbreviation see Figure 1.

ACKNOWLEDGMENTS

We thank Yuping Shi for performing the chromatographic analyses. This work was funded by the University of La Plata through the 11/X 279 Project. S. Martini is a doctoral fellow and M.L. Herrera is an Associate Researcher of the National Research Council of Argentina (CONICET).

REFERENCES

1. Swaisgood, H.E., Characteristics of Edible Fluids of Animal Origin: Milk, in *Food Chemistry*, 1st edn., edited by O.R. Fennema, Marcel Dekker, New York, 1985, pp. 791–828.
2. Kaylegian, K.E., and R.C. Lindsay, Application of Milk Fat Fractions in Foods, in *Handbook of Milkfat Fractionation Technology and Application*, AOCS Press, Champaign, 1995, pp. 525–630.
3. Kellens, M., Developments in Fractionation Techniques, in *Treatise on Fats, Fatty Acids and Oleochemicals*, edited by O.P. Narula, Industrial Consultants, India, 1997, Section B1, Chapter 7, p. 15.
4. Roy, S., and D.K. Bhattacharyya, Comparative Nutritional Quality of Palm Stearin Liquid Oil Blends and Hydrogenated Fat (vanaspati), *J. Am. Oil Chem. Soc. 73*:617–622 (1996).
5. Pal, P.K., D.K. Bhattacharyya, and S. Ghosh, Modifications of Butter Stearin by Blending and Interesterification for Better Utilization in Edible Fat Products, *Ibid. 78*:31–36 (2001).
6. Ng, W.L., and C.H. Oh, A Kinetic Study on Isothermal Crystallization of Palm Oil by Solid Fat Content Measurements, *Ibid. 71*:1135–1139 (1994).
7. Herrera, M.L., M. de León Gatti, and R.W. Hartel, A Kinetic Analysis of Crystallization of a Milk Fat Model System, *Food Res. Internat. 32*:289–298 (1999).
8. Herrera, M.L., C. Falabella, M. Melgarejo, and M.C. Añón, Isothermal Crystallization of Hydrogenated Sunflower Oil: II. Growth and Solid Fat Content, *J. Am. Oil Chem. Soc. 76*:1–6 (1999).
9. Wright, A.J., R.W. Hartel, S.S. Narine, and A.G. Marangoni, The Effect of Minor Components on Milk Fat Crystallization, *Ibid. 77*:463–475 (2000).
10. Herrera, M.L., and R.W. Hartel, Effect of Processing Conditions on Crystallization Kinetics of a Milk Fat Model System, *Ibid. 77*:1177–1187 (2000).
11. Lund, P., Butterfat Triglycerides, *Milchwissenschaft 43*: 159–161 (1988).
12. AOCS, *Official Methods and Recommended Practices of the American Oil Chemists' Society,* 4th edn., American Oil Chemists' Society, Champaign, 1989, Method Cd 16-81.
13. Avrami, M., Kinetics of Phase Change: II. Transformation–Time Relations for Random Distribution of Nuclei, *J. Chem. Phys. 8*: 212–224 (1940).
14. Box, G.E.P., W.G. Hunter, and J.S. Hunter, *Statistics for Experimenters*, John Wiley & Sons, New York, 1978, pp. 208–244.
15. Hartel, R.W., *Crystallization in Foods*, Aspen, Gaithersburg, Maryland, 2001.
16. Martini, S., M.L. Herrera, and R.W. Hartel, Effect of Cooling Rate on Nucleation Behavior of Milk Fat–Sunflower Oil Blends, *J. Agric. Food Chem. 49*:3223–3229 (2001).
17. Breitschuh, B., and E.J. Windhab, Parameter Influencing Co-crystallization and Polymorphism in Milk Fat, *J. Am. Oil Chem. Soc. 75*:897–904 (1998).
18. Graydon, J.W., S.J. Thorpe, and D.W. Kirk, Determination of the Avrami Exponent for Solid State Transformations from Non-isothermal Differential Scanning Calorimetry, *J. Non-Cryst. Solids 175*:31–43 (1994).
19. Christian, J.W., *The Theory of Tranformations in Metals and Alloys,* 2nd edn., Pergamon Press, London, 1975.
20. Martini, S., M.L. Herrera, and R.W. Hartel, Effect of Processing Conditions on Microstructure of Milk Fat Fractions/Sunflower Oil Blends, *J. Am. Oil Chem. Soc. 79*:1063–1068 (2002).

[Received June 7, 2001; accepted August 8, 2002]